

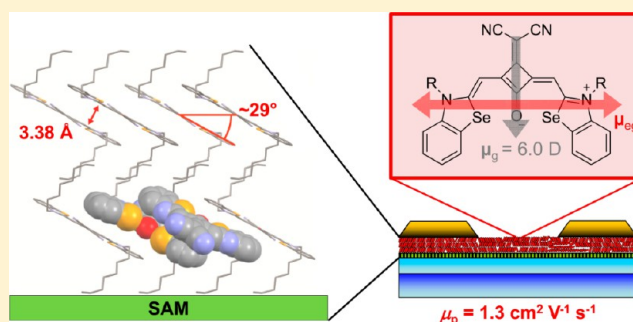
High-Performance Organic Thin-Film Transistors of J-Stacked Squaraine Dyes

Marcel Gsänger,[†] Eva Kirchner,[†] Matthias Stolte,[†] Christian Burschka,[†] Vladimir Stepanenko,[†] Jens Pflaum,[‡] and Frank Würthner^{*,†}

[†]Institut für Organische Chemie and Center for Nanosystems Chemistry, Universität Würzburg, and [‡]Experimentelle Physik VI, Universität Würzburg and Bavarian Center for Applied Energy Research (ZAE Bayern e.V.), Am Hubland, 97074 Würzburg, Germany

S Supporting Information

ABSTRACT: We have synthesized a series of dipolar squaraine dyes that contain dicyanovinyl groups as acceptor and benzannulated five-membered ring heterocycles with alkyl chains of varied length as donor moieties. Based on these squaraines, thin-film transistors (TFT) were fabricated by spin coating and solution shearing. Moreover, with one of these squaraine derivatives vacuum-deposited TFTs were prepared as well. Our detailed studies revealed that the transistor performance of the present series of squaraines is strongly dependent on their structural features as well as on the processing method of thin films. Thus, solution-sheared OTFTs of selenium squaraine bearing dodecyl substituents (denoted as **Se-SQ-C₁₂**) performed best with a maximum hole mobility of $0.45 \text{ cm}^2 \text{ V}^{-1} \text{ s}^{-1}$, which is by far the highest value yet reported for OTFTs based on squaraines. This value was even surpassed by vacuum-deposited thin films of *n*-butyl-substituted selenium squaraine **Se-SQ-C₄**, the only sublimable compound in this series, exhibiting a record hole mobility of $1.3 \text{ cm}^2 \text{ V}^{-1} \text{ s}^{-1}$. Furthermore, we have investigated the morphology of the thin films and the molecular packing of these squaraine dyes by optical spectroscopy, atomic force microscopy, and X-ray diffraction. These studies revealed a relationship between the molecular structure, packing motif, thin-film morphology, and transistor performance of the squaraine dyes. From the supramolecular point of view two packing features discovered in the single crystal structure of **Se-SQ-C₈** are of particular interest with regard to the structure–functionality relationship: The first is the slipped and antiparallel π -stacking motif which ensures cancellation of the molecules' dipole moments and J-type absorption band formation in thin films. The second is the presence of $\text{CN}\cdots\text{Se}$ noncovalent bonds which show similarities to the more common halogen-bonding interactions and which interconnect the individual one-dimensional slipped π -stacks, thus leading to two-dimensional percolation pathways along the source–drain direction.



INTRODUCTION

Vast advancement has been made in the past decade in developing organic semiconductor materials that approach or even surpass the charge carrier mobility of hydrogenated amorphous silicon. Such organic semiconductors have been successfully implemented in a variety of electronic devices such as organic thin-film transistors (OTFTs),¹ photovoltaic cells,² and light-emitting diodes,³ thus gaining increasingly more importance in modern electronics. Small organic molecule-based semiconductor layers have been widely used to constitute the active transport channel of OTFTs,¹ and a few n- and p-type materials have been reported with remarkably high charge carrier mobilities beyond the generally considered bench mark of $1 \text{ cm}^2 \text{ V}^{-1} \text{ s}^{-1}$. For example, a naphthalene diimide (NDI) derivative has been reported to exhibit electron mobilities of about $6 \text{ cm}^2 \text{ V}^{-1} \text{ s}^{-1}$ in vacuum-deposited OTFTs in air.⁴ On the side of p-type semiconductor materials, recently record hole mobilities of up to $8 \text{ cm}^2 \text{ V}^{-1} \text{ s}^{-1}$ have been reported for vacuum-deposited thin films of alkyl-substituted dinaphtho[2,3-*b*:2',3'-*f*]-thieno[3,2-*b*]thiophene.⁵ Among the small organic molecules also

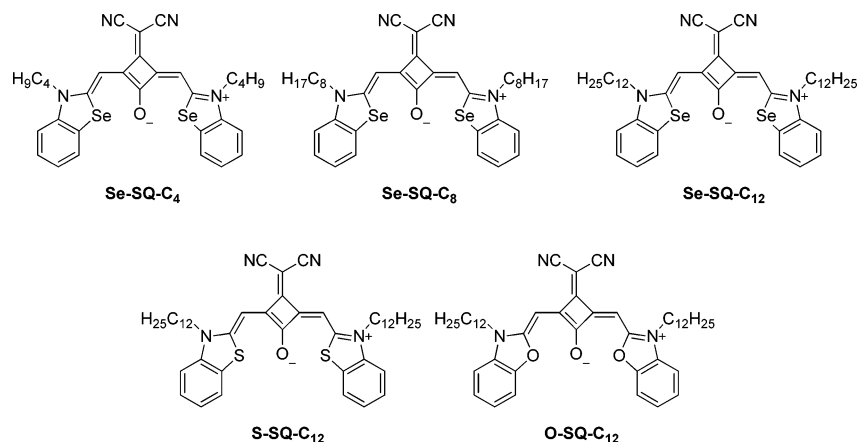
several classes of organic colorants were reported to be potent semiconductor materials in OTFTs besides their classical use for coloring of textiles, paper, food, hair, and so forth. For example, the semiconducting behavior of phthalocyanines was demonstrated already in 1948,⁶ and intensive studies on their application in OTFTs have evolved since then, revealing hole mobilities of up to $3.2 \text{ cm}^2 \text{ V}^{-1} \text{ s}^{-1}$ for vanadium phthalocyanines.⁷ Furthermore, arylene diimides,⁸ diketopyrrolopyrroles,⁹ thienoacenes,¹⁰ and merocyanines¹¹ have been successfully applied in transistor devices.

Besides above-mentioned well-studied classes of colorants, several others are known to possess semiconductivity in thin films but so far were rarely applied in OTFT devices. Squaraines are such a class of dyes which are well-known for their strong absorption and emission in the long-wavelength region accompanied by a remarkable (photo)stability under ambient conditions.^{12,13} They were successfully used as gas sensors,¹⁴ in

Received: September 19, 2013

Published: January 17, 2014

Chart 1. Chemical Structures of the Squaraine Dyes Applied in This Work



bioimaging probes,¹⁵ for photodynamic therapy, in nonlinear optics,¹⁶ and many further applications.^{13,17} In particular, squaraine dyes were applied as highly potent p-type semiconductor materials in xerographic photoconductors¹⁸ and organic solar cells.¹⁹ However, their applicability in OTFT devices has yet been explored rather sporadically. Pagani, Marks, Facchetti, and co-workers reported hole mobilities in the range of 10^{-4} $\text{cm}^2 \text{V}^{-1} \text{s}^{-1}$ for transistor devices based on squaraine derivatives.^{19a} Similar values were reported for squaraines, which were designed for near-infrared light-emitting ambipolar organic field-effect transistors,²⁰ nanowire transistors,²¹ and NIR detectors.²² OTFTs with hole mobilities of around 10^{-3} $\text{cm}^2 \text{V}^{-1} \text{s}^{-1}$ were obtained for the first two cases by spin coating, while in the latter well-aligned and single crystalline squaraine nanowires were used as the active layer of transistor devices ($\mu_p = 2.8 \times 10^{-4}$ $\text{cm}^2 \text{V}^{-1} \text{s}^{-1}$). Acceptor-substituted squaraines were found to exhibit power conversion efficiencies (PCE) of up to 1.8% in bulk heterojunction solar cells.^{19c,g} Spin-coated OTFTs of these dipolar dyes yielded low hole mobilities up to 1.3×10^{-3} $\text{cm}^2 \text{V}^{-1} \text{s}^{-1}$.

Nowadays, demand for TFTs deposited on flexible polymeric substrates has grown for advanced applications such as flexible displays²³ or radiofrequency identification (RFID) tags.²⁴ Thus, deposition methods are required that allow cheap processing of large-scale thin films on flexible substrates. Drop casting²⁵ and spin coating²⁶ are two commonly used techniques allowing fast and easy solution processing of semiconductor thin films. However, these techniques often afford only amorphous films with rather modest transistor performance and are not the methods of choice for large-scale application. Accordingly, alternative solution processing methods such as inkjet printing,²⁷ zone casting,²⁸ and solution shearing²⁹ have been developed to afford more homogeneous films at lower materials consumption.

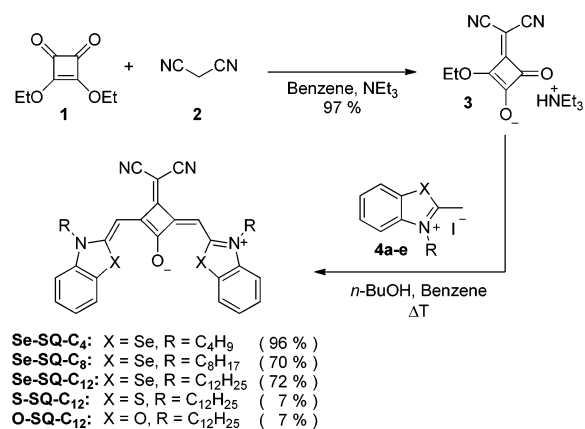
Solution shearing deposition technique, initially developed by Z. Bao and co-workers,^{29a} has been shown to attain higher film quality and better control of film morphology than, e.g., spin coating and hence affords superior transistor performance. As mentioned before, up to now only very moderate mobilities were achieved for squaraine-based OTFTs. Therefore, we approached the question whether the OTFT performance of properly designed squaraine derivatives can be improved by the solution shearing deposition method. Indeed, our detailed studies with the squaraine dyes (shown in Chart 1) revealed that solution-sheared OTFTs of selenium squaraine **Se-SQ-C₁₂** exhibit a hole mobility of $0.45 \text{ cm}^2 \text{V}^{-1} \text{s}^{-1}$, which is by far the highest to date

reported charge carrier mobility for squaraine dyes and one order of magnitude higher than the mobility ($0.039 \text{ cm}^2 \text{V}^{-1} \text{s}^{-1}$) obtained for spin-coated thin films of this squaraine. This value could be even surpassed by vacuum-deposited OTFTs of the squaraine derivative with shorter alkyl chains **Se-SQ-C₄**, exhibiting a mobility of $1.3 \text{ cm}^2 \text{V}^{-1} \text{s}^{-1}$ which can match with that of amorphous silicon. Furthermore, by using optical spectroscopy, atomic force microscopy (AFM), and X-ray diffraction techniques we were able to establish reliable relationships between molecular structure, packing motif in the solid state, thin-film morphology, and transistor performance of the present squaraines.

RESULTS AND DISCUSSION

Synthesis. The dicyano acceptor-substituted squaraine dyes **X-SQ-C_n** ($n = 4, 8, 12$ for $X = \text{Se}$; $n = 12$ for $X = \text{S}, \text{O}$) were synthesized according to the route shown in Scheme 1.³⁰ The

Scheme 1. Synthetic Route to the Acceptor-Substituted Squaraines Investigated in This Work



condensation of squaric acid diethylester (**1**) with malononitrile (**2**) afforded the dicyano acceptor-functionalized squaric acid derivative (**3**), the latter was subsequently reacted with the respective benzoselenazol, benzothiazol, or benzooxazol donors to obtain the desired squaraine derivatives. The synthesis and absorption properties of squaraine dye **Se-SQ-C₁₂** have been reported previously,³⁰ while the remaining squaraines are unknown and, accordingly, were fully characterized by NMR and UV/vis spectroscopy, high-resolution mass spectrometry,

Table 1. Electrical Properties of OTFT Devices of Squaraine Dyes Prepared by Spin Coating from Chloroform Solutions on Si/SiO₂ Substrates and Measured in Air

squaraine	thermal treatment ^{a,b}	$\mu_{p,max}$ [cm ² V ⁻¹ s ⁻¹]	μ_p^c [cm ² V ⁻¹ s ⁻¹]	I_{on}/I_{off}^c	V_{th}^c [V]
Se-SQ-C ₄	^a		no field effect		
	^b	0.0017	0.0016 ± 0.0001	10 ¹	24 ± 1
Se-SQ-C ₈	^a	0.0045	0.0042 ± 0.0003	10 ¹	22 ± 5
	^b	0.0120	0.011 ± 0.001	10 ²	16 ± 2
Se-SQ-C ₁₂	^a	0.018	0.017 ± 0.001	10 ²	16 ± 5
	^b	0.039	0.037 ± 0.001	10 ⁴	6 ± 1
S-SQ-C ₁₂	^a	0.0006	0.00054 ± 0.00004	10 ¹	58 ± 4
	^b	0.0780	0.073 ± 0.005	10 ²	11 ± 1
O-SQ-C ₁₂	^a		no field effect		
	^b		no field effect		

^aWithout annealing. ^bAnnealing of the thin film under argon at 130 °C for 10 min. ^cAverage value of three randomly picked devices.

and, in suitable cases, also by elemental analyses (for details see the Supporting Information).

Spin-Coated OTFT Devices. We have first investigated the performance of TFT devices employing the present series of squaraines by applying the conventional spin-coating method for thin-film deposition on Si/SiO₂ substrates (for details see the Supporting Information). Characterization of the electrical properties of the devices was performed under ambient conditions by measuring at least three devices for each squaraine to obtain averaged values. The hole mobility in the saturation regime was calculated in the usual manner from the slope of the square root of drain current (I_d)^{1/2} vs gate voltage (V_g).^{1a} We observed that for as-cast (without annealing) thin films of selenium-containing squaraines **Se-SQ-C_n** ($n = 4, 8, 12$) the mobility increases with increasing alkyl chain length (C_n), and thus the derivative with the longest alkyl chain (**Se-SQ-C₁₂**) performed best with a hole mobility of 0.017 cm² V⁻¹ s⁻¹, whereas the butyl-substituted squaraine **Se-SQ-C₄** even failed in transistor operation (see Table 1). Thus, to assess the effect of heteroatoms on the electrical properties of squaraines we have investigated the spin-coated thin films of the corresponding dodecyl-substituted sulfur- and oxygen-containing squaraines **S-SQ-C₁₂** and **O-SQ-C₁₂** under identical conditions. For the sulfur derivative **S-SQ-C₁₂** an about two orders of magnitude lower mobility value compared with that of **Se-SQ-C₁₂** was observed, while the oxygen derivative **O-SQ-C₁₂** did not show any field effect.

Annealing of the active layers prior to contact deposition resulted in significant enhancement of the transistor performance compared with that of as-cast thin-film devices for all **Se-SQ-C_n** compounds. More impressively, the mobility of **S-SQ-C₁₂** was increased from 5×10^{-4} cm² V⁻¹ s⁻¹ for as-cast thin-film devices to 0.073 cm² V⁻¹ s⁻¹ after annealing (Table 1). Output and transfer characteristics of an annealed thin film of **Se-SQ-C₁₂** are shown in Figure S1 as an example. Interestingly, upon annealing operating transistor devices were obtained for the butyl-substituted squaraine **Se-SQ-C₄**, which did not show a detectable mobility for as-cast thin films. For **O-SQ-C₁₂**, annealed thin films again did not show any field effect. Thermal annealing also improved the on/off ratio of the drain current by up to two orders of magnitude with a maximum value for I_{on}/I_{off} of 10⁴ for annealed thin films of **Se-SQ-C₁₂**. Threshold voltages in the positive regime and relatively high off-currents of about 10⁻⁸ A were measured for all of these OTFTs. Partially this could be attributed to the high lying HOMO levels of the studied squaraines ($E_{HOMO} = -4.8$ eV, determined by cyclic voltammetry measurements; see Table S4) and the resulting sensitivity to

ambient oxidation or may also be related to doping. Such phenomenon has been systematically studied for freshly prepared pentacene-based thin films with similar high ionization potential ($E_{HOMO} = -5.0$ eV)³¹ upon exposure to air and moisture, where the significant increase of the off-current leads to a rapid decay of the on/off ratio by down to four orders of magnitude with finally almost failing transistor operation.³²

Solution-Sheared OTFT Devices. Next, we investigated the performance of squaraine-based OTFTs produced by the solution-shearing method,²⁹ as the latter is known to attain higher film quality and better control on the morphology than spin coating. We have adapted this method, initially developed by Z. Bao and co-workers,^{29a} to our needs and found that introduction of a tilting angle θ between shearing tool and substrate is beneficial for slow crystallization leading to the formation of large-scale (>2.25 cm²), high-quality thin films. A schematic illustration of our solution shearing setup is shown in Figure 1, and the experimental details are given in the Supporting

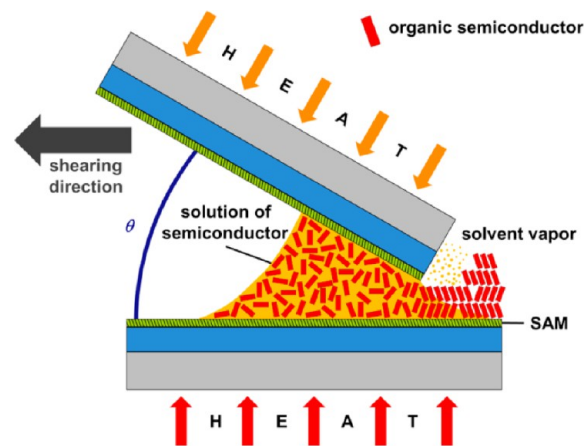


Figure 1. Schematic depiction of the solution-shearing method with relevant processing parameters and information on heat supply, substrate, and shearing tool modifications by SAM layers.

Information. As discussed before, spin-coated OTFTs of dodecyl chain bearing squaraine derivatives showed comparatively better transistor performance than devices of derivatives with shorter alkyl chains. Thus, we have processed thin films of **Se-SQ-C₁₂**, **S-SQ-C₁₂**, and **O-SQ-C₁₂** by solution shearing under ambient conditions and characterized their electrical properties. As sufficient solubility ($c = 2$ mg mL⁻¹) in the high boiling solvent

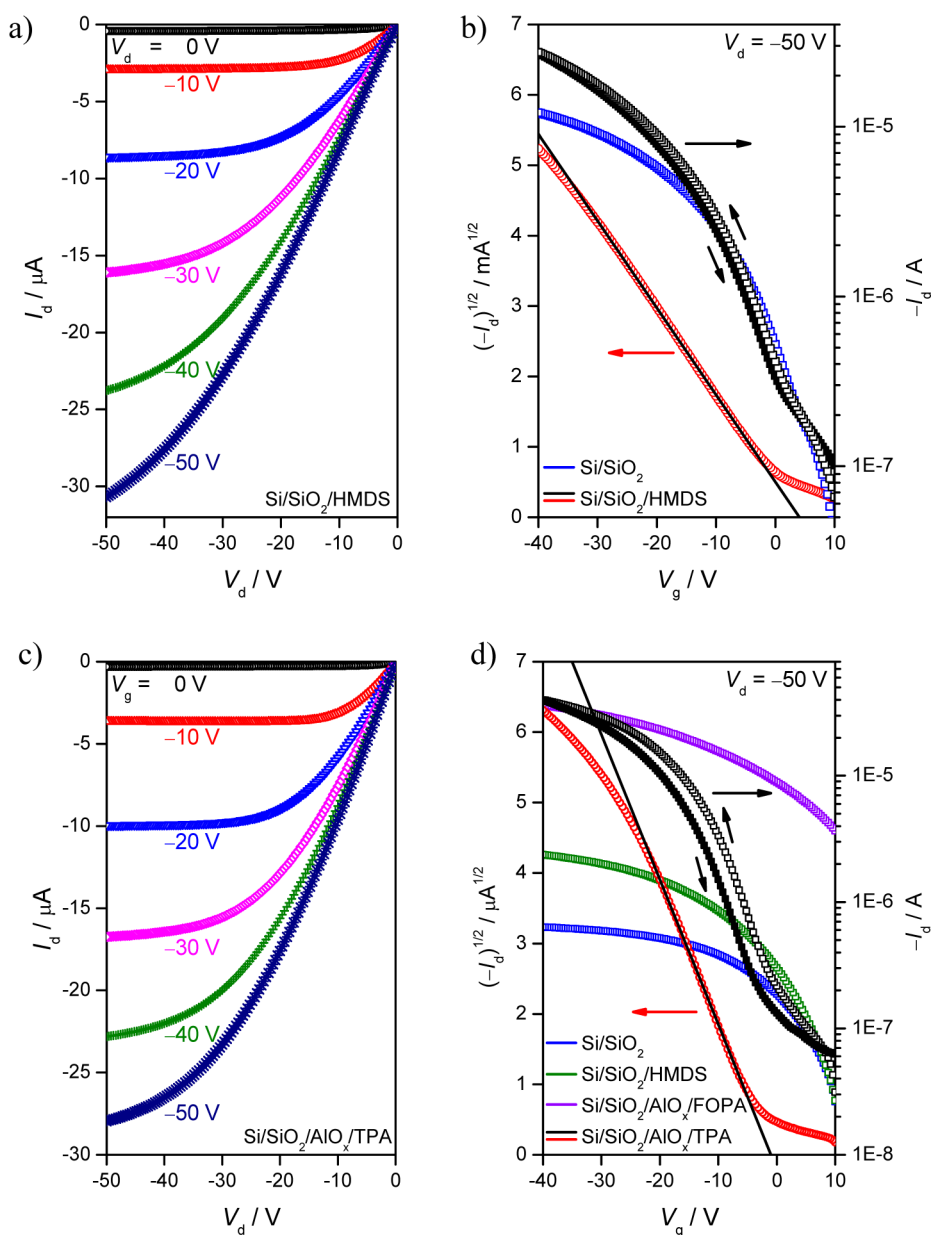


Figure 2. Output (a,c) and transfer (b,d) characteristics of bottom-gate, top-contact OTFTs of solution-sheared squaraine dye **Se-SQ-C₁₂** (a,b) and vacuum-deposited **Se-SQ-C₄** (c,d) on different substrates measured under ambient conditions.

o-dichlorobenzene (*o*-DCB) is required for deposition by solution shearing, we proceeded our investigations with the most soluble squaraine derivatives bearing dodecyl chains.

Interestingly, in contrast to spin-coated thin films of **O-SQ-C₁₂**, its solution-sheared OTFTs counterparts exhibit moderate mobilities with $\mu_{p,max}$ in the range of $1 \times 10^{-4} \text{ cm}^2 \text{ V}^{-1} \text{ s}^{-1}$. For the devices of **S-SQ-C₁₂** quite similar mobilities were observed for both solution-sheared and spin-coated thin films. More pleasingly, for the selenium derivative **Se-SQ-C₁₂** one order of magnitude higher mobilities ($\mu_{p,max} = 0.21 \text{ cm}^2 \text{ V}^{-1} \text{ s}^{-1}$) along the shearing direction, i.e., in so-called parallel orientation, were observed compared to those of as-cast spin-coated OTFTs.

Self-assembled monolayers (SAM) are known to be useful for the optimization of the interface between semiconductor and dielectric, leading to reduced surface energies, less charge trapping, and improved film morphology.^{1d} Thus, we have introduced a monolayer of HMDS in a solution-sheared device of previously best performing **Se-SQ-C₁₂** and, indeed, achieved an

even higher mobility $\mu_{p,max}$ of $0.45 \text{ cm}^2 \text{ V}^{-1} \text{ s}^{-1}$ with an on/off ratio of 10^3 . Output and transfer characteristics of such an OTFT are shown in Figure 2a,b. The high off current could be related to the high lying HOMO levels of the squaraines and OTFT operation under ambient conditions.³² As shown in Table 2, the preferred current flow direction of all solution-sheared devices was found to be parallel to the shearing direction, and devices with their channel in this direction showed up to one order of magnitude higher charge carrier mobilities than those with perpendicular orientation. Representative optical polarization microscopy (OPM) images of **Se-SQ-C₁₂**-based devices on a HMDS-modified substrate are depicted in Figure 3, where the field effect mobilities for 32 transistor devices (20 with parallel and 12 with perpendicular orientation with respect to the shearing direction) are visualized by a color code (Figure 3a). The anisotropy in the OTFT performance is evident from this illustration. The OPM images also hint at preferred growth directions accompanied by a high crystallinity of the **Se-SQ-C₁₂**

Table 2. Ambient Electrical Properties of OTFTs Based on Squaraine Dyes Prepared by Solution Shearing (SS) from *o*-DCB Solution on Si/SiO₂ ($\theta = 15^\circ$) and with HMDS SAM Coverage ($\theta = 0^\circ$)

squaraine	orientation ^a	$\mu_{p,max}$ [cm ² V ⁻¹ s ⁻¹]	μ_p^b [cm ² V ⁻¹ s ⁻¹]	I_{on}/I_{off}^b	V_{th}^b [V]
O-SQ-C ₁₂		0.00015	0.00012 ± 0.00004	10 ²	7 ± 3
	⊥	0.00011	0.00010 ± 0.00001	10 ²	6 ± 4
S-SQ-C ₁₂		0.050	0.017 ± 0.020	10 ¹	54 ± 19
	⊥	0.006	0.003 ± 0.002	10 ¹	57 ± 20
Se-SQ-C ₁₂		0.21	0.15 ± 0.05	10 ³	11 ± 8
	⊥	0.020	0.007 ± 0.008	10 ²	16 ± 3
Se-SQ-C ₁₂ ^c		0.45	0.37 ± 0.06	10 ³	5 ± 1
	⊥	0.12	0.11 ± 0.01	10 ³	5 ± 1

^aOrientation of TFTs with respect to the direction of shearing is symbolized by || (for parallel) and ⊥ (for perpendicular). ^bAverage value of at least three devices. ^cProcessed on HMDS SAM covered SiO₂ substrates.

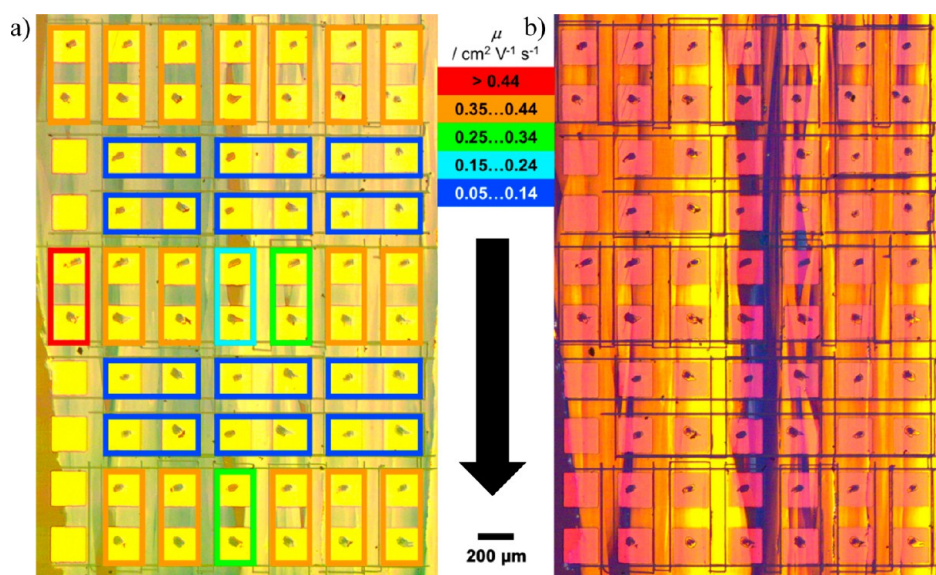


Figure 3. (a) Bright-field optical microscopic and (b) cross-polarized optical microscopic images of thin films prepared by solution shearing of squaraine dye Se-SQ-C₁₂ on Si/SiO₂/HMDS. The overlay for (a) represents the field effect mobilities of 32 TFTs (20 parallel and 12 perpendicular with respect to the shearing direction). The direction of shearing is indicated by the arrow.

Table 3. Electrical Properties of OTFTs of Squaraine Dye Se-SQ-C₄ Prepared by Vacuum Deposition on Different Substrate/SAM Combinations

substrate	SAM	$\mu_{p,max}$ [cm ² V ⁻¹ s ⁻¹]	μ_p^a [cm ² V ⁻¹ s ⁻¹]	I_{on}/I_{off}^a	V_{th}^a [V]
Si/SiO ₂	–	0.016	0.011 ± 0.003	10 ¹	18 ± 2
Si/SiO ₂	HMDS	0.045	0.036 ± 0.005	10 ²	14 ± 2
Si/SiO ₂ /AlO _x	FOPA	0.27	0.23 ± 0.02	10 ¹	30 ± 1
Si/SiO ₂ /AlO _x	TPA	1.3	1.2 ± 0.1	10 ³	–1.2 ± 0.1

^aAveraged over at least three devices.

thin films as they show extended ribbon-like structures along the shearing direction (Figure 3b).

Vacuum-Deposited OTFT Devices. As solution-processed devices of selenium squaraines stand out against those of sulfur and oxygen analogues, we have decided to investigate OTFTs of selenium squaraines by vacuum deposition since this is a traditional, widely used method for the fabrication of smooth and highly crystalline thin films with usually better performance compared to the respective solution-processed counterparts. We could prepare vacuum-deposited thin films only for Se-SQ-C₄, whereas sublimation of the derivatives with longer alkyl chains (C₈ and C₁₂) failed due to decomposition at elevated temperatures. Thermogravimetric analysis of the selenium squaraines shown in Figure S2 indeed revealed higher thermal stability

for the butyl-substituted squaraine Se-SQ-C₄ compared to C₈ and C₁₂ alkyl chain bearing derivatives. The performance of vacuum-deposited OTFTs of Se-SQ-C₄ is summarized in Table 3, and respective *I*–*V* curves are shown in Figure 2c,d.

Devices on bare Si/SiO₂ substrates exhibited p-type charge carrier mobility of 0.016 cm² V⁻¹ s⁻¹, which is about one order of magnitude higher than that of the corresponding spin-coated and annealed ones. Introduction of a HMDS SAM on the Si/SiO₂ substrates improved the transistor performance only slightly to 0.045 cm² V⁻¹ s⁻¹. However, a dramatic increase of mobilities to 0.27 and 1.3 cm² V⁻¹ s⁻¹ was observed by using Si/SiO₂/AlO_x substrates modified with 12,12,13,13,14,14,15,15,16,16,17,17,18,18,18-pentadecylfluoro octadecylphosphonic acid (FOPA) and tetradecylphosphonic acid (TPA), respectively.

By its surface corrugation the SAM has a crucial impact on the quality and morphology of the subsequent semiconducting film, especially on the initial layers where the percolation pathways are formed. Therefore, the enhanced effective charge carrier mobilities obtained within the series of SAMs from HMDS over FOPA to TPA can be rationalized. This is by far the highest value yet obtained for the charge carrier mobility of a squaraine dye and accordingly proves the suitability of these dyes for OTFT applications. For the latter devices we also note improved on/off ratios and a threshold voltage close to zero which support the notion that high film quality also reduces the effect of ambient oxidants or unintentional doping on the transistor performance even for such small bandgap (see below) semiconductors.

Our detailed studies with OTFTs of the present series of squaraine dyes have clearly shown that the transistor performance is dependent, on the one hand, on the electronic nature of the squaraines (i.e., whether they contain Se, S or O atom) and, on the other hand, on the chain length of the alkyl substituents. Selenium squaraines (**Se-SQ-C_n**) performed much better than the corresponding sulfur and oxygen derivatives, and the alkyl chains determine how the materials can be processed. Accordingly dodecyl-substituted **Se-SQ-C₁₂** proved to be most suitable for solution-shearing, while **Se-SQ-C₄** was the material of choice for deposition by sublimation in vacuum. To rationalize our OTFT results, we performed further experiments by UV/vis/NIR spectroscopy, AFM, and X-ray diffraction aiming at relating transistor performance to the packing arrangements of squaraines in thin films.

UV/vis/NIR Spectroscopy Studies. In our previous work we characterized the UV/vis/NIR absorption properties of various dicyanovinyl-substituted squaraine dyes in solution in great detail and confirmed the cisoid molecular scaffold shown in Scheme 1 by single crystal analyses.³⁰ In addition we applied electro-optical absorption measurements (EOAM)³³ to determine the ground- (μ_g) and excited-state (μ_e) dipole moments and the relative polarization of the optical transitions with respect to the molecules' dipole moment. These studies were extended for **Se-SQ-C₁₂** in 1,4-dioxane solution. All results were in line with our earlier conclusions, and accordingly only the outcome will be presented here, while the technical details of our analysis can be found in the Supporting Information and in our previous publication.³⁰ Accordingly, the most prominent absorption band occurring at 727 nm can be attributed to an electronic transition between HOMO and LUMO with presumably CT character, whereas the band at around 400 nm relates to a higher energy transition from the HOMO-1 to the LUMO level.

Evaluation of the EOA spectra under consideration of the C_{2v} symmetry of **Se-SQ-C₁₂** reveals that these transitions are polarized perpendicularly with respect to each other (Figure S3). For the 727 nm band in dioxane the transition dipole moment μ_{eg} is polarized along the long molecular axis, whereas the transition dipole moment related to the short wavelength band μ_{eg} (400 nm) is oriented along the short axis interconnecting the oxygen donor with the dicyanovinyl acceptor of the squaric acid unit which is also the direction of the ground-state dipole moment μ_g . The value for the latter was determined from the EOAM analysis to be 6.0 D.

With this information on the UV/vis/NIR properties of the **Se-SQ-C₁₂** molecule, we have studied the optical properties of thin films processed by different deposition techniques to reveal the molecules' orientation and the excitonic coupling between the molecules' transition dipole moments. UV/vis/NIR spectra of spin-coated and subsequently annealed thin films of squaraines on quartz substrates show significant red shifts for

the lowest-energy transition as compared to those of squaraine monomers in solutions (Figure S4). This unambiguous signature of J-type excitonic coupling^{19g,34} in the thin-films can be attributed to the presence of extended π -stacks organized in a slipped packing arrangement and at close π - π stacking distances. The rather pronounced broadening of the long wavelength bands observed for these thin films appears to arise from static disorder, i.e., inhomogeneous local packing arrangements and/or size of the respective aggregates.³⁵⁻³⁷

Annealing of the thin films by applying the same conditions as for OTFT devices induced only slight changes in the absorption spectra of the selenium squaraines **Se-SQ-C_n** ($n = 4, 8, 12$) (Figure S4a-c). A pronounced sharpening was, however, observed for the long wavelength band of **S-SQ-C₁₂**-based thin films, where also the high-energy transition increases in intensity (Figure S4d) and the shape of the spectrum became almost identical to that of the corresponding selenium derivative **Se-SQ-C₁₂**. These spectral changes can be explained by the enhanced ordering and intermolecular coupling of the squaraine entities, thereby corroborating the dramatic increase of the charge carrier mobility of **S-SQ-C₁₂**-based OTFTs reaching values similar to those of **Se-SQ-C₁₂** upon annealing. In contrast, the different shape and less red-shift of the lowest-energy band of as-cast films of **O-SQ-C₁₂** (Figure S4e) indicate a different, possibly more tilted molecular orientation that is unfavorable for charge transport, as is evident from the OTFT data shown in Table 1. Annealing of these thin films resulted in drastic spectral changes evoked by a phase transition as observed by DSC analysis in the region around 100 °C. However, the attained molecular packing is adverse for transistor operation as the annealed OTFTs of **O-SQ-C₁₂** failed in device operation.

Because of the observed spatial anisotropy in OTFT performance for solution-sheared devices we furthermore recorded UV/vis/NIR spectra of solution-sheared thin films of **Se-SQ-C₁₂** on quartz substrates using linearly polarized light to elucidate a possible correlation of optical and charge transport anisotropy. Similarly to spin-coated films, we observed a bathochromic shift of the absorption maximum in comparison to monomeric solutions accompanied by band broadening. As can be seen from the spectra in Figure 4, rotation of the polarization axis of the incident light from parallel ($\alpha = 0^\circ$) to perpendicular orientation ($\alpha = 90^\circ$) with respect to the shearing

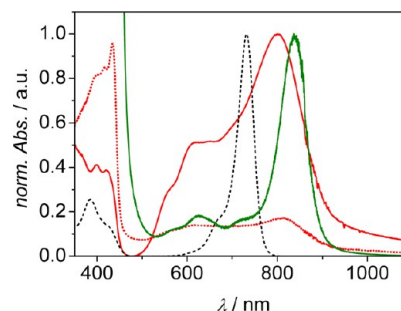


Figure 4. Normalized UV/vis/NIR absorption spectra of squaraine dye **Se-SQ-C₁₂** in *o*-DCB solution (black, dashed) and of its solution sheared thin film (red). The thin-film absorbance was measured with linearly polarized light oriented parallel (red solid; $\alpha = 0^\circ$) and perpendicularly (red dotted; $\alpha = 90^\circ$) with respect to the shearing direction. For comparison, the normalized UV/vis/NIR absorption spectrum (green) of a vapor-deposited thin film of **Se-SQ-C₄** on a Si/Al/ AlO_x /TPA substrate is also shown. This absorption spectrum was calculated from the reflection spectrum by applying the theory of Kubelka and Munk.³⁸

direction caused a dramatic drop of the intensity of the long-wavelength band. This can be attributed to the almost parallel alignment of the transition dipole moment and accordingly the long molecular axis of the molecules (see EOAM results above) to the direction of shearing.

It is also evident from these spectra that the intensity of the second absorption band at shorter wavelengths shows a reversal in intensity for parallel and perpendicularly polarized light, in perfect agreement with its orthogonal orientation.

With regard to the OTFT performance of dodecyl-substituted squaraines (shown in Table 2) it becomes clear that charge transport is favored by extended π -stacks with a slipped packing arrangement along the direction of shearing as indicated by the J-type excitonic coupling. The degree of orientation could be estimated by calculation of the dichroic ratio D_λ and the correlated order parameter S_λ for a band at the wavelength λ .³⁹ A dichroic ratio D_{801} and an order parameter S_{801} are calculated as 5.9 and 0.62, respectively. Calculations for the maximum at 434 nm provide values of $D_{434} = 3.0$ and $S_{434} = 0.40$. For comparison, D values of about 2.2 up to 15 ($S \sim 0.29$ up to 0.82) for liquid crystals^{39a,b} and of 41 ($S = 0.93$) for oligo(*p*-phenylenevinylene)s^{39c} were found after deposition onto rubbed polymer aligned layers. This implies that the application of quite simple solution-shearing method afforded thin films of **Se-SQ-C₁₂** with a high degree of uniaxial alignment explaining the anisotropic charge-transport behavior. In contrast, spin-coated thin films of **Se-SQ-C₁₂** showed no dependence of the UV/vis/NIR absorption spectra upon variation of the polarization of the incident light (Figure S5). This means a random orientation of the molecules and therefore of the transition dipole moments coincides with a lower transistor performance as compared to the well-oriented solution-sheared thin films.

As indicated by the narrow, red-shifted absorption band (shown in green color in Figures 4 and S6), vacuum-deposited thin films of **Se-SQ-C₄** on TPA-modified substrates exhibit a sharper and even more red-shifted J-band³⁴ due to less disorder which explains that these films showed the highest OTFT performance (μ_p up to $1.3 \text{ cm}^2 \text{ V}^{-1} \text{ s}^{-1}$) within our study. This sharp band is indeed unique to films on SAM-modified substrates, whereas a broad absorption band at long wavelengths is observed for the vacuum-deposited thin film of **Se-SQ-C₄** on quartz similar to the spectra of the related solution-casted thin films (Figure S6). Thus, the lower performance of vacuum-deposited thin films on bare Si/SiO₂ substrates (μ_p about $0.01 \text{ cm}^2 \text{ V}^{-1} \text{ s}^{-1}$) can be attributed to a higher degree of disorder, i.e., presence of smaller J-coupled domains which are broader (owing to structural inhomogeneity of the sample) and exhibit smaller red-shifts (owing to smaller sizes of the coherently ordered domains).³⁵

AFM Studies. While our UV/vis/NIR analysis provided valuable information about the microscopic packing arrangement of the squaraine dye molecules, a more macroscopic view on the crystallinity and order of the squaraine thin films can be obtained by AFM analysis. Here again huge differences in the thin-film growth for the different deposition methods were observed. Solution-sheared thin films of **Se-SQ-C₁₂** on bare and HMDS-modified substrates show quite similar topographies (Figure 5) with extended ribbons oriented along the shearing direction and comparable smoothness (RMS = 0.4 nm and 0.8–1.2 nm, respectively). These remarkable large-scale textures were found to cover the whole channel ($L = 100 \mu\text{m}$) between source and drain contact of the transistor device in accordance to the fact that the thin films on HMDS-modified Si/SiO₂ substrates exhibit

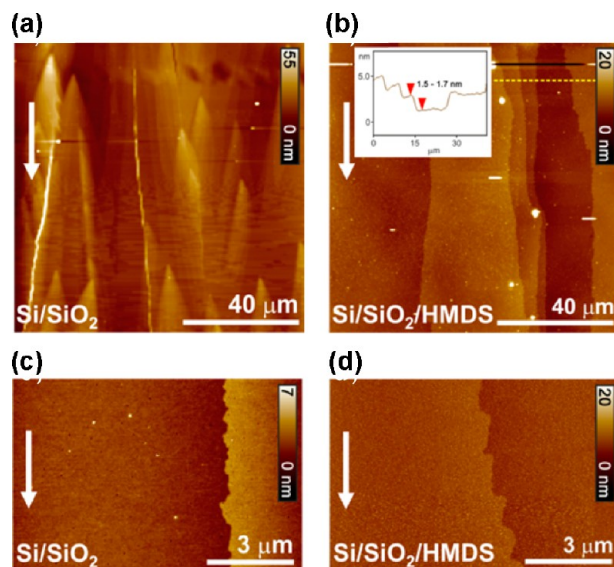


Figure 5. AFM topography images of thin films prepared by solution shearing of squaraine dye **Se-SQ-C₁₂** on Si/SiO₂ (a,c) and on Si/SiO₂/HMDS (b,d). The inset in (b) depicts the height-profile analysis along the yellow dashed line. The direction of shearing is indicated by the arrows.

higher crystallinity and extended grain size (Figure 5b). A layer-by-layer structure was observed by height-profile analysis of the thin film on a HMDS-modified Si/SiO₂ wafer with the height of each step in the range of 1.5–1.7 nm (Figure 5b), which matches the dimension of the molecules. In comparison, AFM images of spin-coated films of **Se-SQ-C₄**, **Se-SQ-C₈**, and **Se-SQ-C₁₂** (Figure S7) reveal more textured and rougher surfaces (RMS roughness between 1.0 and 4.0 nm). Annealing had almost no influence on the morphology. Some larger crystallites were only observed for **Se-SQ-C₁₂**-based thin films after annealing but exhibit still a huge number of grain boundaries. Larger crystallites with extended 3D growth were observed for vacuum-deposited thin films of **Se-SQ-C₄** both on bare (Figure S8a) and on HMDS-modified Si/SiO₂ substrates (Figure S8b). Corresponding thin films on FOPA-modified Si/SiO₂/AlO_x substrates were much more homogeneous showing large domains with few grain boundaries and extended 3D growth (Figure S8c). As shown by the AFM

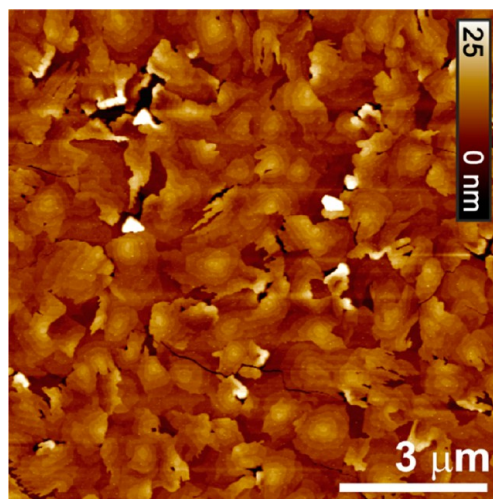


Figure 6. AFM topography image of a thin film prepared by vacuum deposition of squaraine dye **Se-SQ-C₄** on Si/SiO₂/AlO_x/TPA substrate.

comparison of Figures 6 and S8, Si/SiO₂/AlO_x substrates coated by a TPA SAM led to the largest crystalline domains within the series of substrates utilized for vacuum deposition. As the underlying growth dynamics are expected to be substantially different for solution and vacuum deposition, a comparison of the resulting topography by AFM can only be of qualitative nature and might not be conclusive. Therefore, the increase in the effective charge carrier mobility for TPA-modified substrates in respect to HDMS is rather related to the fact that the formation of percolation pathways at the dielectric interface is strongly supported by the quality of the TPA SAM, in particular, its corrugation rather than to the lateral extension of the crystalline domains in respect to HMDS. The surface of the domains features terrace-like structures with a height of 1.5–1.9 nm for each layer (Figure S8d) similar to the values found for solution-sheared films of Se-SQ-C₁₂.

The observed transistor characteristics of Se-SQ-C₁₂ for different deposition techniques correlate well with the respective film morphologies. Thus, low hole mobilities up to 0.04 cm² V⁻¹ s⁻¹ were found for the rough and amorphous spin-coated films, while preparation by solution shearing produced well-oriented, crystalline thin films resulting in one order of magnitude higher hole mobilities (see Table 2). As mentioned before, the vacuum-deposited OTFTs of Se-SQ-C₄ on bare and HMDS-modified Si/SiO₂ substrates showed field-effect mobilities in the range of 0.01–0.04 cm² V⁻¹ s⁻¹, which can be attributed to a 3D growth in these films, being unfavorable for efficient charge transport.⁴⁰ On the other hand, the highly crystalline thin films obtained by

vacuum deposition of Se-SQ-C₄ on FOPA- and TPA-modified substrates resulted in hole mobilities as high as 1.3 cm² V⁻¹ s⁻¹.

Single Crystal X-ray Analysis. To relate charge-transport properties of squaraine dyes to particular noncovalent contacts between the molecular building blocks, single crystal data are needed. Unfortunately, all attempts to grow single crystals of Se-SQ-C₁₂, which performed best in solution-sheared devices, failed. However, we could obtain single crystals of octyl-substituted derivative Se-SQ-C₈ suitable for single crystal X-ray analysis. The molecular structure and the most prominent packing features of this squaraine in solid state are depicted in Figure 7, and the data of the crystal structure are summarized in Tables S1–S3.⁴¹ Remarkably, the packing parallel to the (301) plane (Figure 7a) involves intermolecular CN⋯Se interactions (N–Se distance 3.07 Å) with alternating ribbons of molecules that are separated from one another by a distance of 14.3 Å due to self-segregation induced by the alkyl chains (see Figure 7b). Such CN⋯Se interactions with N–Se-distances between 3.05 and 3.58 Å have been reported before for diselenadiazolyl dimers.⁴² These interactions can be clearly visualized by Hirshfeld analysis⁴³ for Se-SQ-C₈ which pinpoints very close contacts far below van der Waals distances for the CN⋯Se noncovalent bond (see the red points of close contact in Figure 8). The electrostatic character of this noncovalent CN⋯Se interaction has indeed much resemblance to that given in halogen-bonding interactions which have developed into a rapidly growing field of research during the past decade.⁴⁴ Analysis of the molecular packing reveals that the direction of the ground-state dipole moments

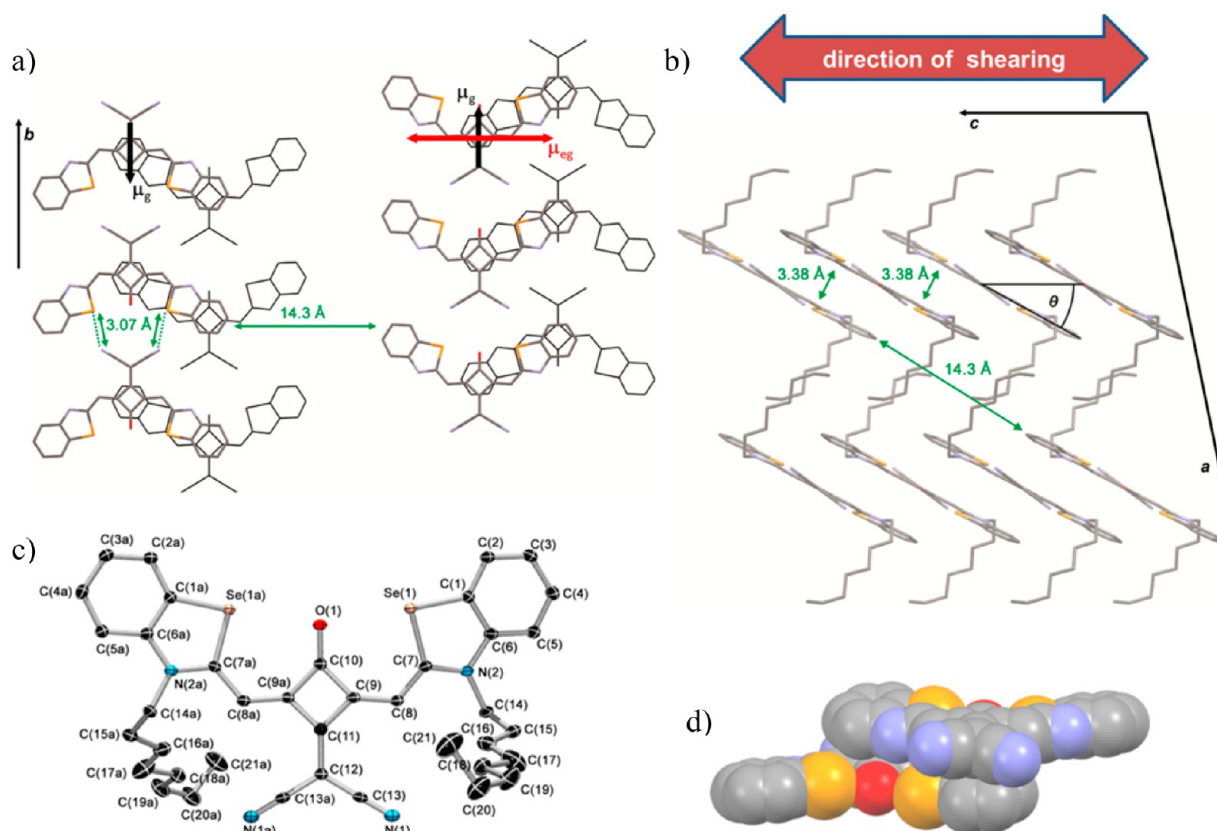


Figure 7. Single crystal X-ray analysis of Se-SQ-C₈. (a) Packing arrangement parallel to the (301) plane with the ground-state and transition dipole moments indicated by black and red arrows, respectively. (b) View onto the (010) plane with definition of the slip angle θ . (c) Molecular structure in the crystal with numbering of the atoms and (d) ball-and-stick model of a centrosymmetric dimer unit of this squaraine dye. Hydrogen atoms (a–d), the octyl chains (a,d) and their disorder (b,c) are omitted for clarity. Thermal ellipsoids are set at 50% probability.

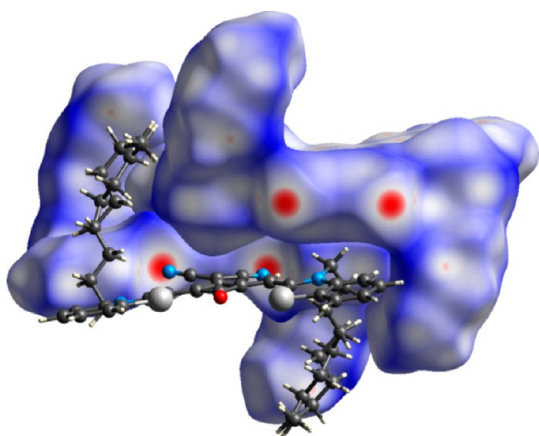


Figure 8. Hirshfeld isoelectric surfaces for two **Se-SQ-C₈** molecules mapped with d_{norm} over the range from -0.224 to 1.55 .⁴³ The view is along the crystallographic b -axis. The color codes are blue, white, and red for distances longer, equal, and shorter than the van der Waals distances of the involved atoms, respectively. A third molecule is shown without the Hirshfeld surface to facilitate visualization of the $\text{CN}\cdots\text{Se}$ interactions.

($\mu_{\text{g}} = 6 \text{ D}$, indicated by the black arrows in Figure 7a) is alternated from ribbon to ribbon, and hence in total the dipole moment is canceled out. Note that a similar antiparallel packing arrangement has been reported to facilitate effective charge transport with hole mobilities of up to $0.18 \text{ cm}^2 \text{ V}^{-1} \text{ s}^{-1}$ for vacuum-deposited devices of a highly dipolar merocyanine.^{11b} The view onto the (010) plane (Figure 7b) reveals furthermore an antiparallel slipped packing arrangement in π -stacks with a close π - π distance of 3.38 \AA . In such an arrangement the transition dipole moments, which were shown to be parallel to the molecules' long axis, are oblique with respect to the (100) plane and show a slip angle θ of about 29° . According to the excitonic coupling theory of Kasha and co-workers,^{36,37} a displacement of the dyes with $\theta < 54.7^\circ$ induces a bathochromic shift of the absorption band (J-coupling). The packing of the two **Se-SQ-C₈** molecules within a centrosymmetric dimeric unit in the solid state is illustrated in Figure 7d. Since the dipole moments of the two molecules point to opposite directions, the molecular ground-state dipole moments are effectively annihilated, which was likewise observed for the packing arrangement parallel to the (301) plane (Figure 7a).

Thin-Film X-ray Diffraction Studies. To link the data derived from the single crystal with the packing in thin films, we performed XRD measurements for solution-sheared films of **Se-SQ-C₁₂**. The specular scans (2θ scans) for spin-coated and solution-sheared OTFT devices on Si/SiO_2 , $\text{Si}/\text{SiO}_2/\text{HMDS}$ and quartz substrates as well as the respective (200) rocking curves for the solution-sheared samples are shown in Figure 9. As can be seen from Figure 9a,b the same crystalline lattice spacing is present for all films independent of the substrate and the processing technique. But significant differences occur in the degree of crystallinity, as indicated by the detectable order of the diffraction spots (Figure 9a: (800) for the solution-sheared films compared to (400) for the annealed and spin-coated samples) as well as by the full-width at half-maximum (fwhm) of the peaks. According to Figure 9a the increase in OTFT performance from as-cast spin-coated films over annealed ones to thin films deposited by solution shearing can be attributed to rising crystallinity in this order. This can be quantified by the highest diffraction order being detectable, by the extension of crystalline grains as deduced from the fwhm as well as by the average angular

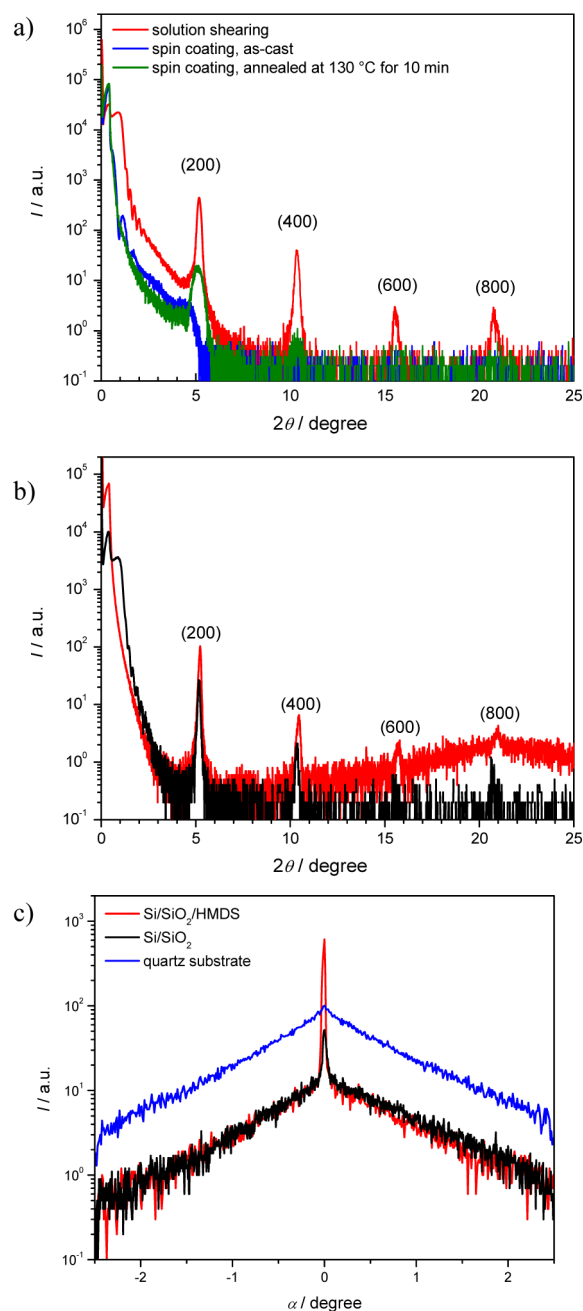


Figure 9. Specular XRD scans of thin films of **Se-SQ-C₁₂** prepared by (a) solution shearing and spin coating on $\text{Si}/\text{SiO}_2/\text{HMDS}$ and (b) solution shearing on Si/SiO_2 (black) and quartz substrates (red). (c) (200) Rocking curves of solution-sheared thin films of **Se-SQ-C₁₂**. The Kissing oscillations (a,b) observed in the angular range up to $2\theta = 1^\circ$ are caused by interference effects of the gold contacts and the SiO_2 layer but not by the organic semiconducting film itself.

tilting of the crystallites (Figure 9c). Since the difference in alkyl chain length of **Se-SQ-C₁₂** and **Se-SQ-C₈** is not that drastic, we assume that the **Se-SQ-C₁₂**-based thin films crystallize in the same space group as found for the single crystals of **Se-SQ-C₈** ($C2/c$). Thus, the observed reflections could be indexed as those arising from the (200), (400), (600), and (800) planes according to the reflection conditions related to this space group.⁴⁵

The (200) rocking curves of **Se-SQ-C₁₂** thin films deposited on different substrates by solution shearing are depicted in Figure 9c. Their peak fwhm is a measure for the angular spread of the orientations of the crystallites with respect to the surface

normal. For films deposited by solution shearing on Si/SiO₂ and Si/SiO₂/HMDS substrates, values of $\pm 0.02^\circ$ were determined, which are indicative of a quite narrow distribution in the domain orientations and, therefore, of a superior angular matching of boundaries within the conduction plane of the transistor device. The peak width increases up to $\pm 0.4^\circ$ for films on quartz substrates. However, these films, which we used for optical spectroscopy, were still a good measure for the thin-film structure of the corresponding OTFT devices as they show nearly identical diffraction patterns (Figure 9b). Thus, one can assume for OTFT devices on Si/SiO₂ similar packing arrangements with the same spatial anisotropy as on quartz.

Packing Model for Thin Films in OTFTs. Our comprehensive characterization of Se-SQ-C_n thin films by X-ray diffraction, polarized UV/vis/NIR spectroscopy, and AFM corroborates the presence of similar dye arrangements for all Se-SQ-C_n dyes on both types of substrates. It is known from EOAM associated with the optical spectroscopy utilizing linearly polarized light that the molecular axis connecting both benzoselenazol units is aligned parallel to the shearing direction (*vide supra*). Assuming that the packing in thin films of Se-SQ-C₁₂ is similar to the molecular arrangement in the crystal structure of Se-SQ-C₈, the crystallographic *c*-axis has to be oriented parallel to the direction of shearing, while the *a*-axis is perpendicular to the substrate surface (Figure 7b). The latter can be deduced from analysis of the (200) Bragg peak of the solution-sheared thin film of Se-SQ-C₁₂ on Si/SiO₂/HMDS (Figure 9a) yielding a layer spacing of 17.1 Å and thus a unit cell parameter *a* of 34.2 Å. This value is about 20% higher as compared to the cell parameter *a* of the crystal structure of Se-SQ-C₈ (27.6 Å), which obviously has to be attributed to the elongation of the alkyl chain from 8 to 12 carbon atoms leading to an increase of the cell parameters with only minor influence on the packing arrangement of the squaraine π -conjugated scaffolds. Additional support comes from the AFM height-profile analysis of solution-sheared thin films of Se-SQ-C₁₂ on Si/SiO₂/HMDS substrates, based on which a layer height of 1.5–1.7 nm could be calculated. This is about half the value of the unit cell parameter *a*-determined by the XRD experiments, implying two alternating monomolecular layers constituting the unit cell along the *a*-direction. This means that after every second monomolecular layer the packing motif is repeated, which is in good accordance with the crystal data of Se-SQ-C₈.

Consequently, all our experimental data can be related to an orientation of the Se-SQ-C₁₂ molecules in solution-sheared thin films, where the projection of the crystallographic *c*-axis is parallel to the shearing direction and the (010) plane is almost perpendicular to the substrate surface as indicated in Figure 7b, top. For such an arrangement, percolation pathways for charge carriers in the crystallographic *c*-direction are provided by the slipped π -stacking motif, while packing arrangement driven by CN \cdots Se interactions is responsible for the additional contribution to the charge transport along the *b*-direction. This is in good agreement with the observed anisotropy in OTFT performance with higher charge carrier mobility ($\mu_{p,max} = 0.45 \text{ cm}^2 \text{ V}^{-1} \text{ s}^{-1}$) parallel to the shearing direction (projection of the *c*-axis) as compared to lower but still remarkable mobility ($\mu_{p,max} = 0.12 \text{ cm}^2 \text{ V}^{-1} \text{ s}^{-1}$) for devices with perpendicular orientation (*b*-axis). Hence, a new noncovalent interaction based on CN \cdots Se bonding which is similar to halogen bonding has been identified in our study to support charge carrier transport. This interaction, together with the slipped π -stacking motif, enables efficient two-dimensional charge-transport parallel to the (100) plane, i.e.,

parallel to the substrate surface, for Se-SQ-C₁₂ transistors. The remarkable charge carrier mobility up to $1.3 \text{ cm}^2 \text{ V}^{-1} \text{ s}^{-1}$ determined for vacuum-deposited devices of Se-SQ-C₄ can also be explained by such a packing as it is confirmed by the optical and AFM data. Besides J-type coupling of the molecules in the thin films, we found a layer spacing for the terrace-like structures of 1.5–1.9 nm (Figure S8d) fitting well to a layer-by-layer packing arrangement as shown in Figure 7a,b for Se-SQ-C₈.

CONCLUSIONS

We have fabricated and characterized a large number of transistor devices based on thin films of a series of acceptor-substituted squaraines with different donor moieties bearing selenium, sulfur, or oxygen atoms and varying length of alkyl substituents. By applying the spin-coating method the selenium and sulfur squaraines with dodecyl substituents (Se-SQ-C₁₂ and S-SQ-C₁₂) are identified as most suited for solution-processed transistor devices as annealed thin films of these squaraines yielded hole mobilities around $0.1 \text{ cm}^2 \text{ V}^{-1} \text{ s}^{-1}$, which already exceeded the previously reported values for squaraine OTFTs¹⁹ by two orders of magnitude. A positive impact on the OTFT performance was achieved by employing solution-shearing method for the deposition of active layers. Anisotropic hole transport behavior with respect to the shearing direction was observed with three to four times higher mobilities for devices with parallel orientation to the shearing direction than for those aligned perpendicularly, affording a highest mobility value of $0.21 \text{ cm}^2 \text{ V}^{-1} \text{ s}^{-1}$ for a Se-SQ-C₁₂ transistor device. Introduction of a HMDS SAM onto the Si/SiO₂ substrates more than doubled the mobility with an average value of $0.37 \text{ cm}^2 \text{ V}^{-1} \text{ s}^{-1}$ and a peak value of $0.45 \text{ cm}^2 \text{ V}^{-1} \text{ s}^{-1}$. A record hole mobility of $1.3 \text{ cm}^2 \text{ V}^{-1} \text{ s}^{-1}$ for squaraine dyes was achieved with the sublimable, shortest alkyl chain bearing derivative Se-SQ-C₄.

For the thin films obtained by different deposition methods, a slipped π -stack arrangement of the molecules with J-type excitonic coupling proved to be the predominant packing motif. The observed anisotropy for the charge transport in solution-sheared films as well as the better performance as compared to spin-coated ones can be explained based on the favorable orientation of the π -stacks along the shearing direction. The fact that a quite high hole mobility was observed in orthogonal direction was explained by CN \cdots Se interactions which constitute a new motif in the field of organic semiconductor research. Our studies convincingly demonstrate the high potential of squaraine dyes for application in organic thin-film transistor devices. The combination of excellent p-channel mobility with high tinctorial strength suggests further applications of these materials as hole transport layers in planar heterojunction and perovskite solar cells.

ASSOCIATED CONTENT

Supporting Information

Further details on the syntheses, single crystal and thin film X-ray analyses, UV/vis/NIR studies, electro-optical absorption spectroscopy, OTFT device fabrication, and AFM studies. This material is available free of charge via the Internet at <http://pubs.acs.org>.

AUTHOR INFORMATION

Corresponding Author

wuerthner@chemie.uni-wuerzburg.de

Notes

The authors declare no competing financial interest.

ACKNOWLEDGMENTS

We thank Robert Hofmockel, Ute Zschieschang and Hagen Klauk (MPI for Solid State Research, Stuttgart) for the preparation of TPA- and FOPA-modified wafers and helpful discussions. Generous financial support by the Bavarian State Ministry of Science, Research, and the Arts for the Center for Nanosystems Chemistry in the framework of the Collaborative Research Network "Solar Technologies Go Hybrid" and by the DFG research unit FOR1809 is gratefully acknowledged.

REFERENCES

- (1) For recent monographs and reviews on organic transistors, see: (a) *Organic Field-Effect Transistors*; Bao, Z., Locklin, J., Eds.; Taylor and Francis, Boca Raton, FL, 2007; (b) *Organic Electronics II*; Klauk, H., Ed.; Wiley-VCH, Weinheim, Germany, 2012; (c) Zausmühl, J.; Siringhaus, H. *Chem. Rev.* **2007**, *107*, 1296–1323. (d) Braga, D.; Horowitz, G. *Adv. Mater.* **2009**, *21*, 1473–1486. (e) Street, R. A. *Adv. Mater.* **2009**, *21*, 2007–2022. (f) Klauk, H. *Chem. Soc. Rev.* **2010**, *39*, 2643–2666. (g) Dong, H.; Wang, C.; Hu, W. *Chem. Commun.* **2010**, *46*, 5211–5222. (h) Wang, C.; Dong, H.; Hu, W.; Liu, Y.; Zhu, D. *Chem. Rev.* **2012**, *112*, 2208–2267. (i) Mei, J.; Diao, Y.; Appleton, A. L.; Fang, L.; Bao, Z. *J. Am. Chem. Soc.* **2013**, *135*, 6724–6746.
- (2) (a) Roncali, J. *Acc. Chem. Res.* **2009**, *42*, 1719–1730. (b) Walker, B.; Kim, C.; Nguyen, T.-Q. *Chem. Mater.* **2011**, *23*, 470–482. (c) Mishra, A.; Bäuerle, P. *Angew. Chem.* **2012**, *124*, 2060–2109; *Angew. Chem., Int. Ed.* **2012**, *51*, 2020–2067. (d) Lin, Y.; Li, Y.; Zhan, X. *Chem. Soc. Rev.* **2012**, *41*, 4245–4272.
- (3) (a) Kulkarni, A. P.; Tonzola, C. J.; Babel, A.; Jenekhe, S. A. *Chem. Mater.* **2004**, *16*, 4556–4573. (b) Meerheer, R.; Walzer, K.; He, G.; Pfeiffer, M.; Leo, K. *Proc. SPIE* **2006**, *6192*, 61920P/1–61920P/16. (c) Sasabe, H.; Kido, J. *Chem. Mater.* **2011**, *23*, 621–630.
- (4) Shukla, D.; Nelson, S. F.; Freeman, D. C.; Rajeswaran, M.; Ahearn, W. G.; Meyer, D. M.; Carey, J. T. *Chem. Mater.* **2008**, *20*, 7486–7491.
- (5) Kang, M. J.; Doi, L.; Mori, H.; Miyazaki, E.; Takimiya, K.; Ikeda, M.; Kuwabara, H. *Adv. Mater.* **2011**, *23*, 1222–1225.
- (6) Vartanyan, A. T. *Zh. Fiz. Khim.* **1948**, *22*, 769–782.
- (7) Huang, L.; Liu, C.; Qiao, X.; Tian, H.; Geng, Y.; Yan, D. *Adv. Mater.* **2011**, *23*, 3455–3459.
- (8) (a) Zhan, X.; Facchetti, A.; Barlow, S.; Marks, T. J.; Ratner, M. A.; Wasielewski, M. R.; Marder, S. R. *Adv. Mater.* **2011**, *23*, 268–284. (b) Würthner, F.; Stolte, M. *Chem. Commun.* **2011**, *47*, 5109–5115.
- (9) (a) Yanagisawa, H.; Mizuguchi, J.; Aramaki, S.; Sakai, Y. *Jpn. J. Appl. Phys.* **2008**, *47*, 4728–4731. (b) Tantiwivat, M.; Tamayo, A.; Luu, N.; Dang, X.-D.; Nguyen, T.-Q. *J. Phys. Chem. C* **2008**, *112*, 17402–17407. (c) Suraru, S.-L.; Zschieschang, U.; Klauk, H.; Würthner, F. *Chem. Commun.* **2011**, *47*, 1767–1769. (d) Qiao, Y.; Guo, Y.; Yu, C.; Zhang, F.; Xu, W.; Liu, Y.; Zhu, D. *J. Am. Chem. Soc.* **2012**, *134*, 4084–4087. (e) Yoon, W. S.; Park, S. K.; Cho, I.; Oh, J.-A.; Kim, J. H.; Park, S. Y. *Adv. Funct. Mater.* **2013**, *23*, 3519–3524.
- (10) (a) Takimiya, K.; Shinamura, S.; Osaka, I.; Miyazaki, E. *Adv. Mater.* **2011**, *23*, 4347–4370. (b) Zhou, Y.; Liu, W.-J.; Ma, Y.; Wang, H.; Qi, L.; Cao, Y.; Wang, J.; Pei, J. *J. Am. Chem. Soc.* **2007**, *129*, 12386–12387.
- (11) (a) Bürckstümmer, H.; Tulyakova, E. V.; Deppisch, M.; Lenze, M. R.; Kronenberg, N. M.; Gsänger, M.; Stolte, M.; Meerholz, K.; Würthner, F. *Angew. Chem.* **2011**, *123*, 11832–11836; *Angew. Chem., Int. Ed.* **2011**, *50*, 11628–11632. (b) Huang, L.; Stolte, M.; Bürckstümmer, H.; Würthner, F. *Adv. Mater.* **2012**, *24*, 5750–5754.
- (12) Keil, D.; Hartmann, H.; Moschny, T. *Dyes Pigm.* **1991**, *17*, 19–27.
- (13) (a) Sreejith, S.; Carol, P.; Chithra, P.; Ajayaghosh, A. *J. Mater. Chem.* **2008**, *18*, 264–274. (b) Ajayaghosh, A. *Acc. Chem. Res.* **2005**, *38*, 449–459.
- (14) Cox, J. R.; Müller, P.; Swager, T. M. *J. Am. Chem. Soc.* **2011**, *133*, 12910–12913.
- (15) (a) Ohira, S.; Rudra, I.; Schmidt, K.; Barlow, S.; Chung, S. J.; Zhang, Q.; Matichak, J.; Marder, S. R.; Bredas, J. L. *Chem.—Eur. J.* **2008**, *14*, 11082–11091. (b) Chung, S. J.; Zheng, S. J.; Odani, T.; Beverina, L.; Fu, J.; Padilha, L. A.; Biesso, A.; Hales, J. M.; Zhan, X. W.; Schmidt, K.; Ye, A. J.; Zojer, E.; Barlow, S.; Hagan, D. J.; Van Stryland, E. W.; Yi, Y. P.; Shuai, Z. G.; Pagani, G. A.; Bredas, J. L.; Perry, J. W.; Marder, S. R. *J. Am. Chem. Soc.* **2006**, *128*, 14444–14445.
- (16) Jisha, V. S.; Arun, K. T.; Hariharan, M.; Ramaiah, D. *J. Am. Chem. Soc.* **2006**, *128*, 6024–6025.
- (17) For recent reviews on various applications of squaraine dyes: (a) Beverina, L.; Salice, P. *Eur. J. Org. Chem.* **2010**, 1207–1225. (b) Gassensmith, J. J.; Baumes, J. M.; Smith, B. D. *Chem. Commun.* **2009**, 6329–6338. (c) Halton, B. *Chem. N. Z.* **2008**, *72*, 57–62.
- (18) (a) Law, K. Y.; Bailey, F. C. *J. Imaging Sci.* **1987**, *31*, 172–177. (b) Law, K. Y.; Facci, J. S.; Bailey, F. C.; Yanus, J. F. *J. Imaging Sci.* **1990**, *34*, 31–38. (c) Law, K. Y. *Chem. Mater.* **1992**, *4*, 605–611.
- (19) (a) Silvestri, F.; Irwin, M. D.; Beverina, L.; Facchetti, A.; Pagani, G. A.; Marks, T. J. *J. Am. Chem. Soc.* **2008**, *130*, 17640–17641. (b) Bagnis, D.; Beverina, L.; Huang, H.; Silvestri, F.; Yao, Y.; Yan, H.; Pagani, G. A.; Marks, T. J.; Facchetti, A. *J. Am. Chem. Soc.* **2010**, *132*, 4074–4075. (c) Mayerhöffer, U.; Deing, K.; Gruß, K.; Braunschweig, H.; Meerholz, K.; Würthner, F. *Angew. Chem.* **2009**, *121*, 8934–8937; *Angew. Chem., Int. Ed.* **2009**, *48*, 8776–8779. (d) Völker, S. F.; Uemura, S.; Limpinsel, M.; Mingebach, M.; Deibel, C.; Dyakonov, V.; Lambert, C. *Macromol. Chem. Phys.* **2010**, *211*, 1098–1108. (e) Wei, G.; Wang, S.; Sun, K.; Thompson, S. R. *Adv. Energy Mater.* **2011**, *1*, 184–187. (f) Shi, Y. R.; Hill, R. B. M.; Yum, J. H.; Dualah, A.; Barlow, S.; Graetzel, M.; Marder, S. R.; Nazeeruddin, M. K. *Angew. Chem.* **2011**, *123*, 6749–6751; *Angew. Chem., Int. Ed.* **2011**, *50*, 6619–6621. (g) Deing, K. C.; Mayerhöffer, U.; Würthner, F.; Meerholz, K. *Phys. Chem. Chem. Phys.* **2012**, *14*, 8328–8334. (i) Stender, B.; Völker, S. F.; Lambert, C.; Pflaum, J. *Adv. Mater.* **2013**, *25*, 2943–2947.
- (20) Smits, E. C. P.; Setayesh, S.; Anthopoulos, T. D.; Buechel, M.; Nijssen, W.; Coehoorn, R.; Blom, P. W. M.; de Boer, B.; de Leeuw, D. M. *Adv. Mater.* **2007**, *19*, 734–738.
- (21) Zhang, C.; Zhang, X.; Zhang, X.; Ou, X.; Zhang, W.; Jie, J.; Chang, J. C.; Lee, C.-S.; Lee, S.-T. *Adv. Mater.* **2009**, *21*, 4172–4175.
- (22) (a) Binda, M.; Agostinelli, T.; Caironi, M.; Natali, D.; Sampietro, M.; Beverina, L.; Ruffo, R.; Silvestri, F. *Org. Electron.* **2009**, *10*, 1314–1319. (b) Mayerhöffer, U.; Fimmel, B.; Würthner, F. *Angew. Chem.* **2012**, *124*, 168–171; *Angew. Chem., Int. Ed.* **2012**, *51*, 164–167.
- (23) (a) Burrows, P. E.; Forrest, S. R.; Thompson, M. E. *Curr. Opin. Solid State Mater. Sci.* **1997**, *2*, 236–243. (b) MacDonald, W. A. *J. Mater. Chem.* **2004**, *14*, 4–10. (c) Gelinck, G. H.; Huitema, H. E. A.; van Veenendaal, E.; Cantatore, E.; Schrijnemakers, L.; van der Putten, J. B. P. H.; Geuns, T. C. T.; Beenhakkers, M.; Giesbers, J. B.; Huisman, B.-H.; Meijer, E. J.; Benito, E. M.; Touwslager, F. J.; Marsman, A. W.; van Rens, B. J. E.; de Leeuw, D. M. *Nat. Mater.* **2004**, *3*, 106–110. (d) Geffroy, B.; le Roy, P.; Prat, C. *Polym. Int.* **2006**, *55*, 572–582. (e) Ju, S.; Li, J.; Liu, J.; Chen, P.-C.; Ha, Y.-G.; Ishikawa, F.; Chang, H.; Zhou, C.; Facchetti, A.; Janes, D. B.; Marks, T. J. *Nano Lett.* **2008**, *8*, 997–1004.
- (24) (a) Subramanian, V.; Frechet, J. M. J.; Chang, P. C.; Huang, D. C.; Lee, J. B.; Moles, S. E.; Murphy, A. R.; Redinger, D. R.; Volkman, S. K. *Proc. IEEE* **2005**, *93*, 1330–1338. (b) Berggren, M.; Nilsson, D.; Robinson, N. D. *Nat. Mater.* **2007**, *6*, 3–5. (c) Usta, H.; Facchetti, A.; Marks, T. J. *Acc. Chem. Res.* **2011**, *44*, 501–510.
- (25) Gao, X.; Di, C.; Hu, Y.; Yang, X.; Fan, H.; Zhang, F.; Liu, Y.; Li, H.; Zhu, D. *J. Am. Chem. Soc.* **2010**, *132*, 3697–3699.
- (26) Dong, H.; Li, H.; Wang, E.; Wie, Z.; Xu, W.; Hu, W.; Yan, S. *Langmuir* **2008**, *24*, 13241–13244.
- (27) Moonen, P. F.; Yakimets, I.; Huskens, J. *Adv. Mater.* **2012**, *24*, 5526–5541.
- (28) (a) Pisula, W.; Menon, A.; Stepputat, M.; Lieberwirth, I.; Kolb, U.; Tracz, A.; Siringhaus, H.; Pakula, T.; Müllen, K. *Adv. Mater.* **2005**, *17*, 684–689. (b) Mas-Torrent, M.; Masirek, S.; Hadley, P.; Crivillers, N.; Oxtoby, N. S.; Reuter, P.; Veciana, J.; Rovira, C.; Tracz, A. *Org. Electronics* **2008**, *9*, 143–148.
- (29) (a) Becerril, H. A.; Roberts, M. E.; Liu, Z.; Locklin, J.; Bao, Z. *Adv. Mater.* **2008**, *20*, 2588–2594. (b) Giri, G.; Verploegen, E.; Mannsfeld, S.

C. B.; Atahan-Evrenk, S.; Kim, D. H.; Lee, S. Y.; Becerril, H. A.; Aspuru-Guzik, A.; Toney, M. F.; Bao, Z. *Nature* **2011**, *480*, 504–508. (c) Lee, W.-Y.; Oh, J. H.; Suraru, S.-L.; Chen, W.-C.; Würthner, F.; Bao, Z. *Adv. Funct. Mater.* **2011**, *21*, 4173–4181. (d) Stolte, M.; Gsänger, M.; Hofmöckel, R.; Suraru, S.-L.; Würthner, F. *Phys. Chem. Chem. Phys.* **2012**, *14*, 14181–14185.

(30) Mayerhöffer, U.; Gsänger, M.; Stolte, M.; Fimmel, B.; Würthner, F. *Chem.—Eur. J.* **2013**, *19*, 218–232.

(31) (a) Chen, Z.; Müller, P.; Swager, T. M. *Org. Lett.* **2006**, *8*, 273–276. (b) Klauk, H.; Zschieschang, U.; Weitz, R. T.; Meng, H.; Sun, F.; Nunes, G.; Keys, D. E.; Fincher, C. R.; Xiang, Z. *Adv. Mater.* **2007**, *19*, 3882–3887. (c) Nayak, P. K.; Periasamy, N. *Org. Electron.* **2009**, *10*, 1396–1400.

(32) (a) Kim, W. J.; Koo, W. H.; Jo, S. J.; Kim, C. S.; Baik, H. K. *J. Vac. Sci. Technol., B* **2005**, *23*, 2357–2362. (b) Jung, H.; Lim, T.; Choi, Y.; Yi, M.; Won, J.; Pyo, S. *Appl. Phys. Lett.* **2008**, *92*, 163504.

(33) Liptay, W. In *Excited States*; Lim, E. C., Ed.; Academic Press: New York, 1974, Vol. 1, pp 129–229.

(34) Würthner, F.; Kaiser, T. E.; Saha-Möller, C. R. *Angew. Chem.* **2011**, *123*, 3436–3473; *Angew. Chem., Int. Ed.* **2011**, *50*, 3376–3410.

(35) Kistler, K. A.; Pochas, C. M.; Yamagata, H.; Matsika, S.; Spano, F. C. *J. Phys. Chem. B* **2012**, *116*, 77–86.

(36) McRae, E. G.; Kasha, M. *J. Chem. Phys.* **1958**, *28*, 721–722.

(37) Kasha, M.; Rawls, R.; El-Bayoumi, M. A. *Pure Appl. Chem.* **1965**, *11*, 371–392.

(38) Kubelka, P.; Munk, F. *Z. tech. Phys.* **1931**, *12*, 593–601.

(39) (a) West, J. L.; Magyar, G. R.; Kelly, J. R. *Appl. Phys. Lett.* **1995**, *67*, 155–157. (b) Culligan, S. W.; Geng, Y.; Chen, S. H.; Klubek, K.; Vaeth, K. M.; Tang, C. W. *Adv. Mater.* **2003**, *15*, 1176–1180. (c) Nishizawa, T.; Lim, H. K.; Tajima, K.; Hashimoto, K. *J. Am. Chem. Soc.* **2009**, *131*, 2464–2465.

(40) Verlaak, S.; Steudel, S.; Heremans, P.; Janssen, D.; Deleuze, M. S. *Phys. Rev. B* **2003**, *68*, 195409.

(41) Crystallographic data (excluding structure factors) for the structure reported in this paper have been deposited with the Cambridge Crystallographic Data Centre as supplementary publication no. CCDC-956684. Copies of the data can be obtained free of charge from www.ccdc.cam.ac.uk/conts/retrieving.html

(42) Davis, W. M.; Hicks, R. G.; Oakley, R. T.; Zhao, B. *Can. J. Chem.* **1993**, *71*, 180–185.

(43) (a) Wolff, S. K.; Grimwood, D. J.; McKinnon, J. J.; Turner, M. J.; Jayatilaka, D.; Spackman, M. A. *CrystalExplorer*, version 3.0; University of Western Australia: Crawley, Australia, 2012; (b) Spackman, M. A.; Jayatilaka, D. *CrystEngComm* **2009**, *11*, 19–32.

(44) (a) Metrangolo, P.; Pilati, T.; Resnati, G. *CrystEngComm.* **2006**, *8*, 946–947. (b) Metrangolo, P.; Resnati, G.; Pilati, T.; Biella, S. In *Halogen Bonding: Fundamental and Applications*, Springer Book Series: Structure and Bonding; Springer: Berlin, 2008; Vol 126, pp 105–136.

(45) *International Tables for Crystallography*, 5th ed.; Hahn, Th., Ed.; Kluwer Academic Publishers: Dordrecht, The Netherlands, 2002; Vol. A.

■ NOTE ADDED AFTER ASAP PUBLICATION

This paper was published ASAP on January 30, 2014 with incorrect text. Edits were made to clarify the text. The corrected version was reposted on February 3, 2014.